IRIS AperTO

UNIVERSITÀ DEGLI STUDI DI TORINO

AperTO - Archivio Istituzionale Open Access dell'Università di Torino

Hydrothermal preparation of B–TiO2-graphene oxide ternary nanocomposite, characterization and photocatalytic degradation of bisphenol A under simulated solar irradiation

This is the author's manuscript

Original Citation:

Availability:

This version is available http://hdl.handle.net/2318/1769215 since 2021-01-26T16:57:45Z

Published version:

DOI:10.1016/j.mssp.2020.105591

Terms of use:

Open Access

Anyone can freely access the full text of works made available as "Open Access". Works made available under a Creative Commons license can be used according to the terms and conditions of said license. Use of all other works requires consent of the right holder (author or publisher) if not exempted from copyright protection by the applicable law.

(Article begins on next page)

24 November 2026

The published paper (https://doi.org/10.1016/j.mssp.2020.105591) is available at this website:
https://www.sciencedirect.com/science/article/abs/pii/S1369800120315237?via%3Dihub

Hydrothermal preparation of B–TiO_2-graphene oxide ternary nanocomposite, characterization and photocatalytic degradation of bisphenol A under simulated solar irradiation

Ilknur Altin [a,*], Xianzheng Ma [b], Vittorio Boffa [b], Emin Bacaksız [c], Giuliana Magnacca [d]

[a] Department of Chemistry, Faculty of Science, Karadeniz Technical University, 61080, Trabzon, Turkey
[b] Center for Membrane Technology, Department of Chemistry and Bioscience, Aalborg University, Fredrik Bajers Vej 7H, 9220, Aalborg, Denmark
[c] Department of Physic, Faculty of Science, Karadeniz Technical University, 61080, Trabzon, Turkey
[d] Dipartimento di Chimica and NIS Interdepartmental Centre, Universitá di Torino, Via P. Giuria 7, 10125, Torino, Italy

ARTICLE INFO

Keywords:
Graphene oxide
Boron doped TiO_2
Solar induced photocatalysis
Solar simulator
Endocrine disrupting chemical

ABSTRACT

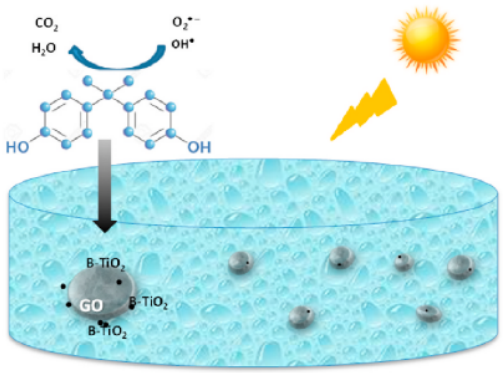
Boron-doped TiO_2 decorated on graphene oxide photocatalysts (denoted as GO@B–TiO_2) were prepared for the effective photocatalytic treatment of bisphenol A (BPA) from water under simulated solar light. To prepare GO@B–TiO_2 nanocomposites, B–TiO_2 was initially synthesized via a sol-gel procedure and subsequently decorated on graphene oxide at 70 °C, by a facile hydrothermal method. Characterization results show that B–TiO_2 particles are anchored on the surface of graphene oxide successfully. Their photocatalytic efficiency could also be adjusted by changing the ratios between B–TiO_2 and GO. The optimum GO loading is 2 wt%, at which GO@B–TiO_2 nanocomposite photocatalyst could achieve the best BPA degradation percentage of 47.66% compared with B–TiO_2 materials (18.78%) after 240 min of solar irradiation. The dominant reactive oxygen species (ROS) formed during the photocatalytic abatement of BPA were determined to be $O_2^{\cdot-}$ and $^{\cdot}OH$. The presence of carbonate and chloride induced moderate inhibitory effect on GO@B–TiO_2 (2 wt% GO), while bicarbonate and nitrate displayed only minor effect towards photocatalytic degradation of BPA. Based on these results, the as-prepared nanocomposites may be used as efficient and promising photocatalysts in secondary treatments to degrade recalcitrant contaminants in water exploiting the visible-light region of the full solar spectrum.

1. Introduction

With the rapid development of technology and economy, various contaminants have been discharged into the environment in recent decades. As a results, the safety of fresh water has become a global concern [1,2]. Endocrine disrupting compounds (EDCs) and their degradation products in water sources can be considered as contaminants of emerging concern (CECs), which adversely affect the environment and the human health. Indeed, EDCs are able to disrupt the activity of hormones by mimicking their chemical structure and blockage the cell receptors in the body [3]. Bisphenol A (2,2-bis (4-hydroxyphenyl) propane, BPA), a well-known endocrine disrupting chemical and highly toxic compound, is widely used in the production of polycarbonate polymers. Its concentration can range from ng L^{-1} to μg L^{-1}level in groundwater, surface water, and wastewater systems [4,5]. It was also reported that BPA has some embryotoxicity and teratogenicity that may increase the risk of ovarian cancer, prostate cancer, asthma and leukemia even in low concentration [6]. Even though some conventional methods such as coagulation, sedimentation, biodegradation have been applied to remove BPA, this pollutant still remains at trace level concentrations (ng L^{-1}) in the treated water [7]. As BPA cannot be removed/degraded thoroughly via conventional water treatment technologies, more efficient, sustainable and cost effective water treatment techniques are required to remove CECs such as BPA. Among the available strategies, semiconductor-mediated photocatalysis, which can function under solar energy to degrade many harmful organic contaminants from wastewater without generating toxic products, is taken into consideration as an encouraging alternative remediation method [8–11].

Heterogeneous photocatalysis method has been widely discussed for

* Corresponding author.
E-mail address: ilknurtatlidil@ktu.edu.tr (I. Altin).



Scheme 1. Schematic structure of graphene-based material for degradation of BPA.

dye degradation, air remediation, water disinfection and decomposing of organic pollutants in the literature [12–14]. Briefly, when TiO_2 is illuminated with appropriate UV light ($\lambda \geq$ band-gap of TiO_2) electron (e^-_{CB}) and positively charged hole (h^+_{VB}) pairs are generated and they can produce ROS such as $OH^{\cdot}$, $O_2^{\cdot-}$ and H_2O_2 on the surface of the TiO_2 catalyst. These oxidizing agents can decompose contaminants of emerging concern (CECs), including endocrine disrupting compounds, which transform into CO_2, H_2O and by-products [15].

TiO_2 semiconductor is widely used because it is considered one of the most efficient photocatalysts, with sustainable properties such as non-toxicity, chemical stability and photo-durability [16,17]. Moreover, TiO_2-based photocatalysts have been shown to be able to mineralize many CECs, included BPA [18–21]. However, the wide band gap energy (~3.2 eV) and the rapid electron-hole recombination limit the usage of pristine TiO_2 in photocatalytic applications. Moreover, when irradiated with solar radiation, its quantum yield is usually low, as it has almost no response to visible light, which hamper TiO_2 application to real-scale systems [22,23]. Many methods, such as doping or co-doping and combination with other narrow band gap semiconductor materials, have been used to increase the photocatalytic efficiency of TiO_2 under visible or sun light irradiation [24]. For instance, doping with foreign atoms such as B, N and F could boost the efficiency of TiO_2-based photocatalysts under the visible light by reducing their band gap energy, thus making them suitable for exploiting sunlight for the abetment of CECs in water systems [25–27]. Boron ions substitute oxygen in the TiO_2 lattice. Hence, by doping with boron *2p* states with oxygen *2p* ones, the valence band (VB) energy edge of the TiO_2 semiconductor is slightly red-shifted. Therefore, B-doping can be used to decrease the band gap energy of TiO_2 and obtain high photocatalytic performance under visible light or sun light irradiation [25].

Even after the changes mentioned above, the photocatalytic activity of TiO_2 is still restrained by its low specific surface area and aggregation. Since the photocatalytic phenomena happen on the surface of photocatalysts, the adsorption of the contaminants at the surface of TiO_2 in the aqueous phase is a key parameter [28]. Recently, a widespread method applied for increasing the activity of catalysts was the immobilization of TiO_2 or other semiconductor nanomaterials on a co-adsorbent nanostructure surface such as metal organic framework, ceramic, alumina, zeolites and carbon-based materials [29,30]. Various research reports have focused on the immobilization of TiO_2 in carbonaceous materials containing activated carbon, carbon nanotubes and graphene [31,32]. In particular, graphene has attracted considerable attentions due to its high electronic carrier mobility, outstanding surface, and particular optical properties [33,34]. Various graphene-semiconductor nanostructured photocatalysts have been reported to enhance the activity of the semiconductor suppressing the aggregation of semiconductor particles [35,36]. Also graphene oxide was used as co-catalyst and support for semiconductors [21,37,38]. Synergistic interaction of the graphene-based material and the semiconductor, can facilitate different steps of the photodegradation process: (i) it can red-shift the range of light absorption for a better exploitation of the solar light; (ii) the excited electrons can be quickly transferred sp^2-hybridized carbon network, thus hindering electron–hole recombining; (iii) the graphene-based material can adsorb pollutants close to the photocatalytic centers, e.g. by π–π stacking (Scheme 1).

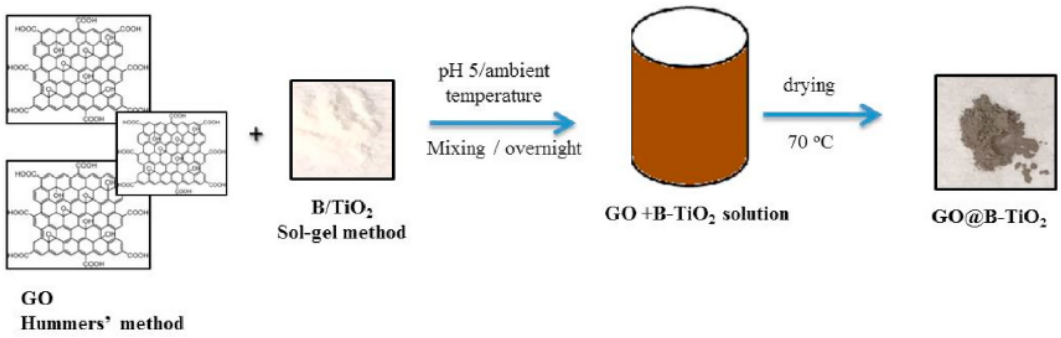
In a study published by Han et al. [37] nitrogen on sulfur co-doped reduced graphite oxide (NS-rGO) had been prepared for anchoring of CdS. The photocatalytic activity of the nanocomposite had been evaluated for hydrogen production and 4-nitrophenol (4-NP) reduction into 4-aminophenol under visible light (300 W Xe lamp, $\lambda \geq 420$ nm). The authors reported that 4-NP was degraded completely with CdS/5% NS-rGO after 6 min photocatalytic reaction. They reported that the nanocomposite had higher photocatalytic efficiency than pure CdS (62%). In another study, Xu et al. [21] investigated the preparation of Ti^{3+} and oxygen vacancies (Ti^{3+}/O_v) self-doped TiO_2 and its mixing in rGO nanocomposite (TiO_{2-x}/rGO) using hydrothermal calcination method. They studied the photocatalytic efficiency of the hybrid catalysts for the degradation of BPA (2.5 mg L^{-1}) and achieved a significant improvement in photocatalytic efficiency of nanocomposite compared to pure TiO_{2-x} or pure TiO_2 under visible light (light intensity = 2000 ± 10 W m^{-2}). In conclusion, the embedding of semiconductors in graphene-structures and doping can introduce synergistic effects improving the harvesting of the solar spectrum, the adsorption ability, and the efficiency of electron-hole separation and transfer processes of TiO_2 photocatalysts. As a consequence, this approach can allow producing high-efficient photocatalytic materials which can be used in scale-up applications.

In present study, an effective two-step procedure was used to prepare B-doped TiO_2 decorated on GO. B–TiO_2 was first synthesized via sol-gel method and subsequently decorated on GO by facile hydrothermal process to prepare GO@B-doped TiO_2 ternary heterojunction photocatalyst. The catalytic activity of the prepared materials was examined towards the degradation of BPA under the solar light. The prepared GO was combined with B–TiO_2 with a loading of 0.5, 1, 2 and 5% by mass (hereinafter defined as 0.5GO@B–TiO_2, 1GO@B–TiO_2, 2GO@B–TiO_2 and 5GO@B–TiO_2, respectively). All the samples were deeply characterized in order to determine the main features of the composite materials. In addition, some more accurate analyses were carried out on the best photocatalyst (namely 2GO@B–TiO_2) in order to evidence the molecular behaviors affecting its activity in the photocatalytic reaction. The same sample was also tested in more complex matrices containing inorganic ions or humic acid in order to assess the behavior of the system in a more real situation (simulated natural water). Moreover, major oxidizing species were also investigated. Reusability of the material was also evaluated for moving to scaled-up applications.

2. Experimental

2.1. Chemicals and materials

Titanium (IV) isopropoxide (99%), absolute ethanol, H_3BO_3 (99%), HCl (36.5%), H_2SO_4 (95%), $NaNO_3$ (99%), $KMnO_4$ (99%), H_2O_2 (35% in water), NaOH (98%), $NaNO_3$ (99%), NaCl (99.5%), Na_2SO_4 (99%), Na_2CO_3 (99%), humic acid sodium salt, acetonitrile (HPLC grade, 99.9%), bisphenol A (97%), isopropyl alcohol (99%), benzoquinone (98%), ethylenediaminetetraacetic acid disodium salt dehydrate (99%), and terephthalic acid (98%) were purchased from Sigma-Aldrich. Graphite powder was bought from Kropfmuhl GmbH, Hauzenberg, Germany. Model solutions were prepared with deionized water (resistivity ≥ 18 MΩ cm), which was obtained by a dedicated laboratory purification system.



Scheme 2. Schematic of the preparation process of GO@B–TiO_2.

2.2. Synthesis of B–TiO_2 nanoparticles

The pristine B–TiO_2 was synthesized using a sol-gel procedure with some modifications [39]. First, 8.4 mL titanium (IV) isopropoxide was dissolved into 20 mL ethanol (mixture A). The mixture was left stirring vigorously for 2 h. Then, 130 mL ethanol containing 0.22 mL conc. HCl, 0.5 mL water and 0.44 g H_3BO_3 (which is equal to 1% of TiO_2 mass) was added dropwise to mixture A and the resulting mixture was kept stirring overnight to yield a wet gel. The above gel mixture was dried at 80 °C for 12 h. After drying process, the final product was calcined at 450 °C for 4 h. Finally, the product was collected from furnace and keep using for further usage.

2.3. Synthesis of graphene oxide (GO) material

Graphene oxide was prepared by graphite powder through a modified Hummers' method [40,41]. Briefly, commercially graphite powder (2 g, Graphit Kropfmuhl GmbH) was mixed with 92 mL of H_2SO_4 (98%) in a flask and $NaNO_3$ (2 g) was added slowly and then stirred for 20 min in an ice bath till it cooled down (~0 °C). Subsequently, 12 g of potassium permanganate ($KMnO_4$) was gradually added with constant stirring for 30 min. The reaction temperature was kept at 35 °C and stirred for 1 h in water bath. After continuous stirring the reaction mixture was heated up to 90 °C in the silicon oil bath and 140 mL of water was added slowly to the mixture left mixing for a further 1 h. Finally, after cooling to RT the mixture, 400 mL of H_2O were added and 14 mL of 30% H_2O_2 were then added dropwise, turning the mixture color into light yellow. After that, the final product was collected, washed with distilled water and centrifuged (10,000 rpm, 10 min 20 °C). Washing and centrifugation procedures were repeated five times. Finally, GO powder could be obtained by drying in a vacuum freeze dryer at −44 °C.

2.4. Synthesis of GO@B–TiO_2 composite

GO@B–TiO_2 composite photocatalysts were prepared by a hydrothermal method with pH control at ambient temperature. A certain amount of GO (which is equal to 0.5, 1, 2% of TiO_2 mass, respectively) was first dispersed into H_2O by ultrasonication for 1 h and pH of the GO suspension was adjusted to 5 with 0.1 M HCl or 0.1 M NaOH solutions. Also 250 mg B–TiO_2 was dispersed into H_2O (10 mL) and sonicated for 1 h. B–TiO_2 and GO suspension were mixed together, kept sonicating

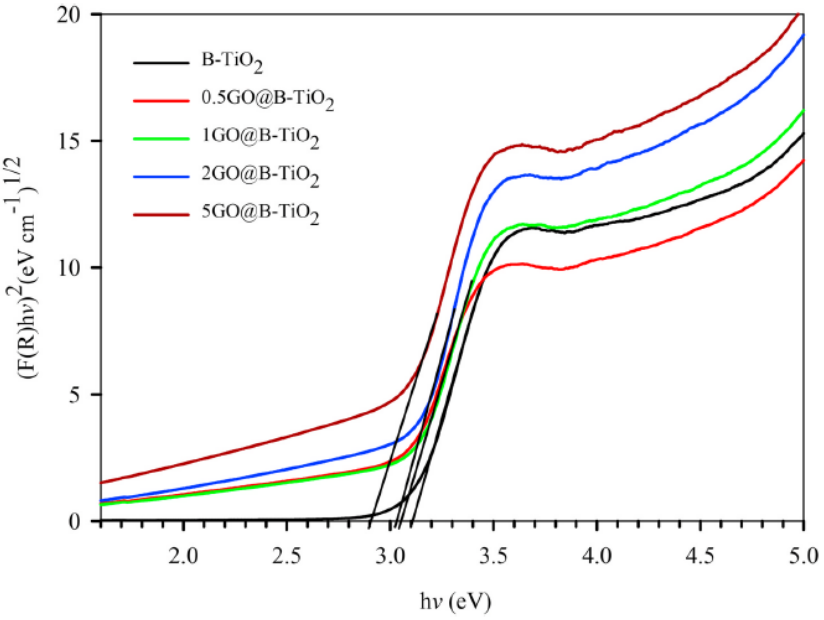


Fig. 1. Optical band gap energies of B–TiO_2 and composites.

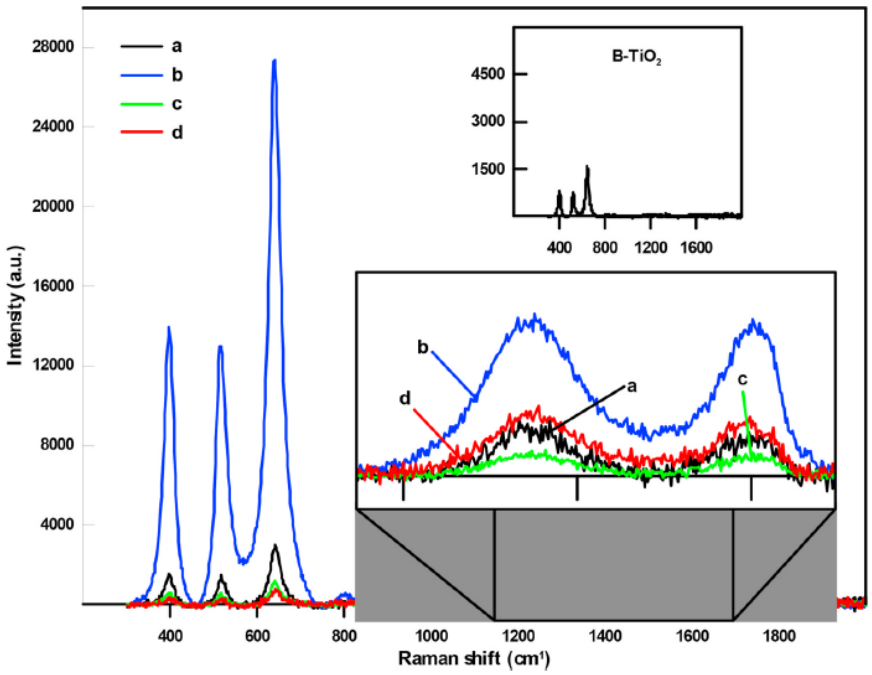


Fig. 2. Raman spectra of B–TiO_2 (inset), 0.5GO@B–TiO_2 (a), 1GO@B–TiO_2 (b), 2GO@B–TiO_2 (c) and 5GO@B–TiO_2 (d).

for 1 h and stirring overnight to get GO@B–TiO_2 composites. Finally, the resulting product was dried in a vacuum oven at 70 °C for further usage (Scheme 2). In this way, we obtained a series of x%GO@B–TiO_2 by adjusting the mass ratios of GO to B–TiO_2 (x = 0, 0.5, 1, 2 and 5). The color of modified samples (0.5GO@B–TiO_2, 1GO@B–TiO_2, 2GO@B–TiO_2 and 5GO@B–TiO_2) were changed from white to gray and dark gray, compared with B–TiO_2 (Scheme 1S).

2.5. Characterization of GO@B–TiO_2 composite

The physical and chemical properties of the as-prepared catalysts were examined by different techniques. Powder X-ray diffraction (XRD, PANanalytical Empyrean diffractometer) of the composites was carried out using CuKα radiation. Surface morphology were analyzed by FIB-SEM Tescan S9000G operating in the range 3–10 keV. The surface components were determined by X-ray photoelectron spectroscopy (XPS, PHI 5000 Versa Probe spectrometer with an Al-Ka radiation source). UV–vis diffused reflectance spectra (DRS) were carried out by a UV-VIS-NIR spectrophotometer (Shimadzu UV-3600 Plus). Raman spectra of the composites were recorded on (Renishaw/Invia). Photo-luminescence (PL) spectra were determined on a fluorescence spectro-photometer (Cary eclipse).

2.6. Photocatalytic experiments

BPA was used to evaluate the photodegradation activity of the composites using a double-walled high borosilicate glass cell under solar simulator. The simulated solar light was produced by a 300 W xenon lamp (1000 W m^{-2} light intensity, model LS0306, LOT Quantum Design, GmbH) and the calibration of the equipment was carried out with a Si reference solar cell (Model LS0042, ReRa System, Netherlands) before photocatalytic experiments. The reaction temperature was maintained at 25 ± 0.1 °C using a thermostatic bath (HAAKE K20). For a typical test, 40 mL of BPA (10 mg L^{-1}) solution was introduced in the photoreactor and 40 mg photocatalyst (to obtain the final concentration of 1 g L^{-1}) was added into the reaction cell. The obtained slurry was sonicated for 5 min to get homogeneous dispersion of photocatalyst, dissolved oxygen and BPA and then the mixture was constantly stirred magnetically during the experiment. The pH values before and after experiments were rather stable at approximately pH 5. Before the light irradiation, the solution mixture containing the catalyst was stirred for 1 h to establish adsorption/desorption equilibrium. During the degradation process, the

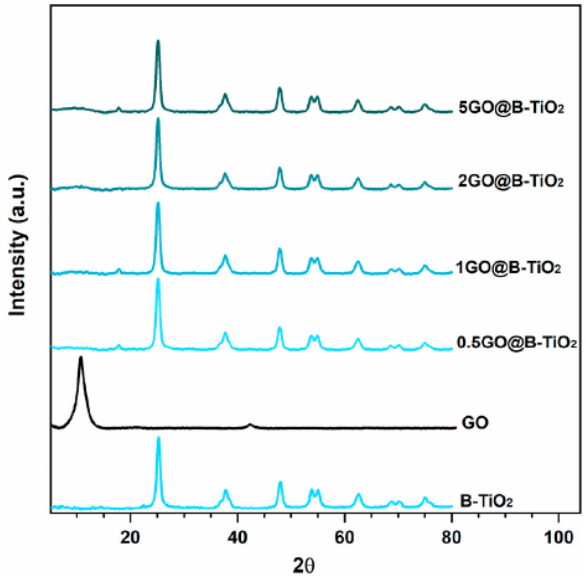


Fig. 3. XRD patterns of the composite samples compared to the signals of pure GO and B–TiO_2.

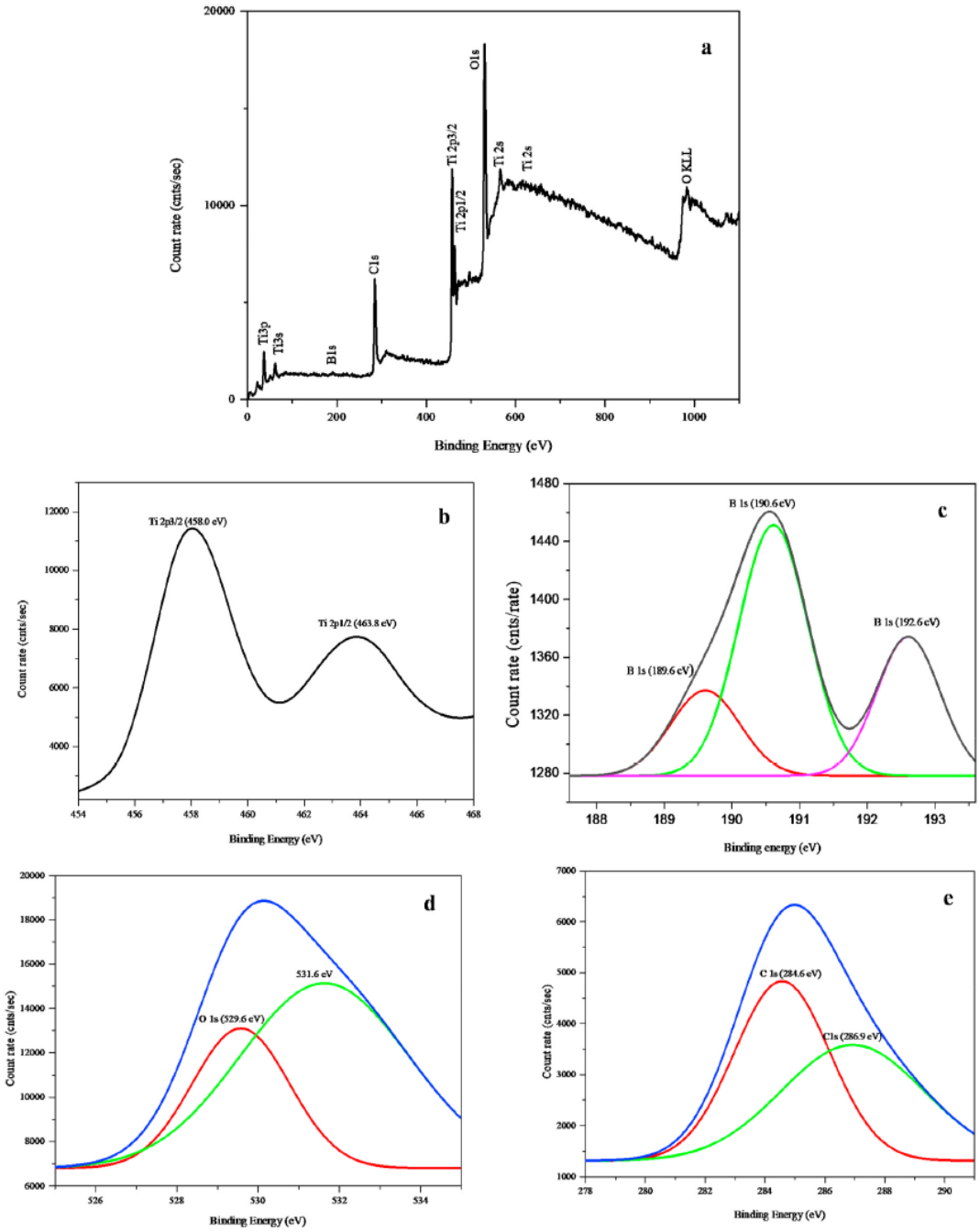


Fig. 4. a) XPS survey spectra of the 2GO@B–TiO_2; the corresponding high resolution XPS spectra of b) Ti 2p, c) B 1s, d) O 1s and e) C 1s.

suspension were sampled at regular intervals of time and centrifuged for 10 min at 5000 rpm. Finally, the centrifuged liquid filtrated using syringe membrane filter (0.45 μm) was analyzed on HPLC and the separated catalyst was simply washed with distilled water and kept to perform reusability tests, then reused in a new photocatalytic cycle under the same degradation conditions. The effect of anions on photocatalytic treatment efficiency of BPA was examined on the best photocatalyst recognized during the photocatalytic tests by introducing $NaNO_3$, NaCl, Na_2SO_4 and Na_2CO_3, respectively. In order to simulate more realistic water, we evaluated also the influence of humic acid presence on the degradation yield. To determine the formation of different ROS during the photocatalytic reaction, ethylenediamine tetra acetic acid (EDTA, a hole scavenger), benzoquinone (BZQ, a O_2^- radical scavenger) and isopropyl alcohol (an ·OH radical scavenger) were added. In addition, the terephthalic acid (TA) PL probing technique was performed to determine the formation of ·OH by the solar light

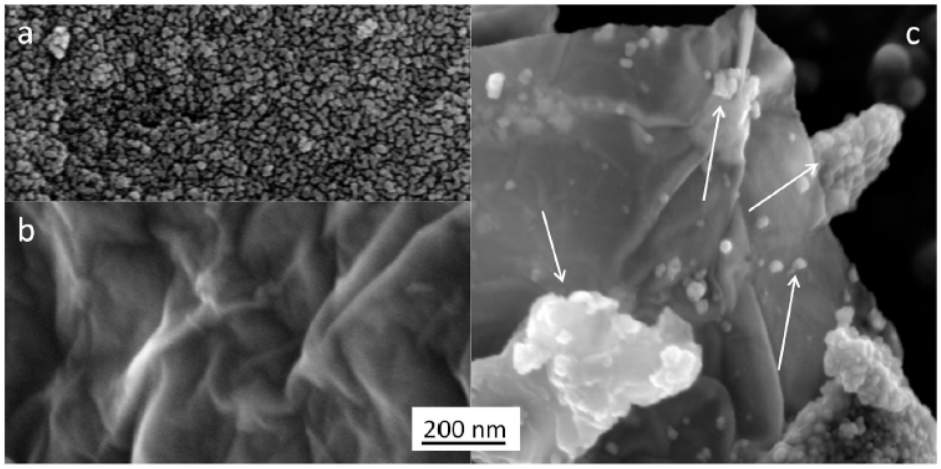


Fig. 5. FIB-SEM images of a) B–TiO_2, b) GO and c) 2GO@B–TiO_2.

irradiated photocatalyst. The remaining amount of BPA was calculated as C_t/C_o, in which C_t was the residual BPA concentration and C_o was the initial BPA concentration. The value of kinetic rate constants was evaluated considering the residual BPA concentration over the scheduled time intervals during the photocatalytic process; the data were fitted by the pseudo-first order model using the following equation:

$$\ln(\frac{Co}{Ct}) = kt \quad (1)$$

The apparent rate constant k (min^{-1}) is the slope of the fitted curve of $\ln(C_o/C_t)$ versus reaction time.

The control experiments were carried out in the absence of light or without photocatalysts to evaluate BPA photolysis. Duplicate tests were performed for each experiment, and the relative standard deviation was found generally less than 5%.

2.7. Analytical methods

The residual BPA concentration was analyzed through the high performance liquid chromatography (HPLC, Dionex with Chromeleon 6.80 software) equipped with C18 column (Kinetex EVO-C18, 4.6 mm × 150 mm, 5 μm) and UV detector (DAD). The conditions were acetonitrile/water (60/40, v/v) at a flow rate of 1.0 mL min^{-1} as eluent and the 230 nm of detector wavelength.

3. Results and discussion

3.1. Structural and morphological analysis

The light absorption capacities of B–TiO_2 and 2GO@B–TiO_2 were examined using UV–vis diffuse reflectance spectroscopy (DRS). As displayed in Fig. 1, neat B–TiO_2 (black curve) showed a strong absorption edge in the UV region at wavelength shorter than 400 nm, indicating B–TiO_2 is near visible UV-light response catalyst, while 2GO@B–TiO_2 showed a broad absorption in the visible region and its absorption extended up to 500 nm. It indicated that the addition of GO enabled the photoactivition of the composite under the visible-light irradiation. The band gap energies (E_g) of B–TiO_2 and GO@B–TiO_2 composites were calculated from Kubelka-Munk equation [42]:

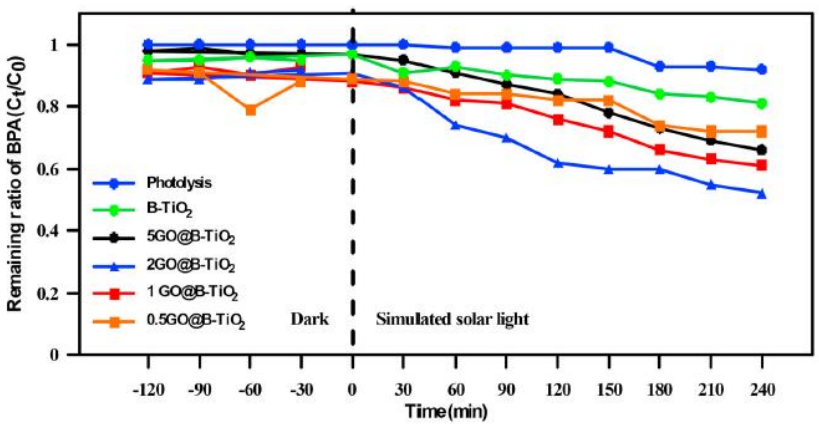
$$F(R) = (1\text{-}R)^2/2R \quad (2)$$

Where R is the diffuse reflectance. According to this equation, the optical band gap energy can be calculated by plotting the $F(R)^2$ vs. the energy in electron volts and then extrapolating the linear part of the curve to $F(R)^2 = 0$. The E_g values were found as 3.10, 3.06, 3.06, 3.02 and 2.90 eV for B–TiO_2, 0.5GO@B–TiO_2, 1GO@B–TiO_2, 2GO@B–TiO_2 and 5GO@B–TiO_2 catalysts, respectively. In addition, a decrease in the band gap of GO@B–TiO_2 is due to hybridization between C 2p and O 2p orbitals which forms an impurity energy level above the valence band [43].

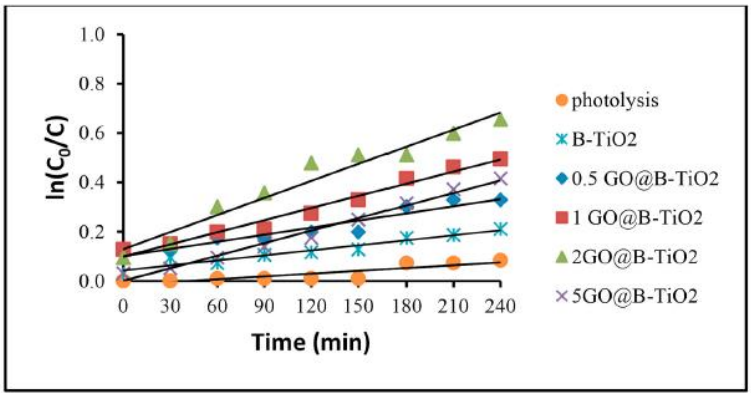
The presence of GO and B-doped TiO_2 is also confirmed using Raman analysis results. Fig. 2 shows the typical peaks of GO@B–TiO_2 at 396 cm^{-1} (B_{1g}), 516 cm^{-1} (A_{1g}) and 639 cm^{-1} (E_g) corresponding to the vibrations of B–TiO_2 [44,45]. In addition, D and G bands at 1356 cm^{-1} and 1587 cm^{-1}, characteristic of GO and attributed to the sp^3 and sp^2 in plane vibrations of bonded carbons [46], were observed in GO@B–TiO_2 composites.

The crystal phase composition of all catalysts was investigated using XRD, whose results were reported in Fig. 3. All materials are crystalline and show the anatase form of TiO_2 with the typical peaks at 25.3°, 37.8°, 48.0°, 54.0°, 55.0°, 62.7°, 68.9°, 70.3° and 75.1°, which were ascribed to the (101), (004), (200), (105), (211), (204), (116), (220) and (211) planes, respectively [47]. The typical peak of GO at 10.7° was not monitored in the XRD patterns of GO@B–TiO_2 catalysts, likely because the amount of GO in GO@B–TiO_2 hybrid composites is quite limited, or because a large fraction of GO sheets in the composite is intercalated by B–TiO_2 nanoparticles and aggregate in a disordered pattern. The intensity of XRD patterns of all materials is nearly similar. The crystalline sizes of B–TiO_2, 0.5GO@B–TiO_2, 1GO@B–TiO_2, 2GO@B–TiO_2, 5GO@B–TiO_2 were calculated by the Scherrer equation [48] from the broadening of (101) reflection as 14.04, 14.50, 15.44, 14.04, 14.05 nm, respectively. In all cases a nanometric dispersion of the B–TiO_2 particles is observed, and this is expected to favor a good interaction GO@B–TiO_2 and a consequent enhanced photoactivity of the composite, higher in the case of 2GO@B–TiO_2 and 5GO@B–TiO_2 which present the smaller crystalline domains.

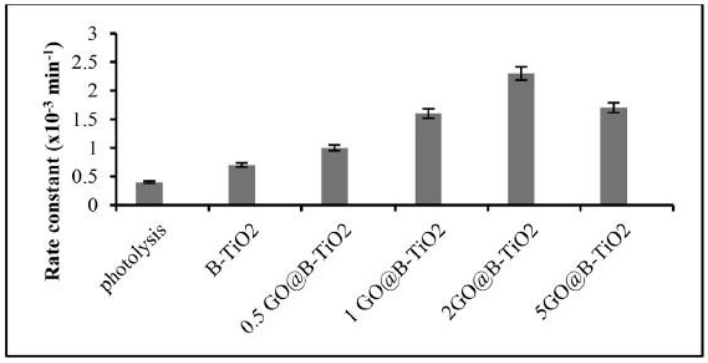
Given the photocatalytic results, a deep characterization of the surface feature was carried out by XPS only on the best photocatalyst, namely 2GO@B–TiO_2. Strong photoelectron peaks of B (*1s*), Ti (*2p*), C (*1s*) and O (*1s*) were monitored on the XPS survey spectrum (Fig. 4a), indicating the expected composition of the composite material. The two peaks of Ti *2p*, reported in Fig. 4b, confirmed the presence of Ti $2p_{3/2}$



a)



b)



c)

Fig. 6. a) Adsorption and photocatalytic degradation of BPA under solar irradiation, b) relation between ln (C_0/C) and time and c) apparent first-order rate constant (k_{app}) [C_0 = 10 mg L^{-1}; Catalyst amount = 1 g L^{-1}; pH 5.0].

Table 1
Kinetic constants and PD efficiencies of catalysts.

Process	Catalyst load ($g\ L^{-1}$)	BPA ($mg\ L^{-1}$)	k ($x10^{-3}$ min^{-1})	R^2	PD[a] at 4 h (%)
Photolysis	-	10	0.4	0.773	8.1
B/TiO_2	1	10	0.7	0.936	18.8
$0.5GO@B/TiO_2$	1	10	1	0.916	28.4
$1GO@B/TiO_2$	1	10	1.6	0.975	38.8
$2GO@B/TiO_2$	1	10	2.3	0.955	47.6
$5GO@B/TiO_2$	1	10	1.7	0.985	33.6

[a] PD: Photocatalytic degradation.

(458.0 eV) and Ti $2p_{1/2}$ (463.8 eV) chemical states with spin orbital splitting of 5.8 eV, typical of Ti^{4+} oxidation state in octahedral configuration, compatible with the anatase structure. No evidence of Ti^{3+} species is evidenced in the spectrum, even if boron is expected to induce the reduction of TiO_2 surface [49]. B1s XPS signal of GO@B–TiO_2 composite, reported in Fig. 4c, can be fitted by two components. The strongest peak at 190.6 eV is associated with boron that is possibly interstitially weaved in the TiO_2 structure with Ti–O–B structure [50]. The second peak at 192.6 eV is related to B–O–B groups, typical of H_3BO_3 or B_2O_3 and low energy peak at 189.6 eV is related to boron incorporated into the TiO_2 lattice through occupying O sites to form O–Ti–B bond [51]. Su et al. also reported that the peak at 189.6 eV might be related to B–Ti in TiB_2 [52] The extension of these domains is expected to be very limited as no XRD signals of crystalline H_3BO_3 or B_2O_3 were observed in Fig. 3. The O 1s XPS spectrum (Fig. 4d) confirms the presence of only two types of oxygen, namely Ti–O–Ti and Ti–O–B at 529.6 and surface hydroxyl groups at 531.6 eV [51]. Finally, the signal in the C1s XPS region is due to carbon impurities and can be fitted by two components, namely at 286.08 eV, assigned to partially oxidised carbonaceous moieties (C–O bonds) [53], and at 284.6 eV, corresponding to C–C bonds, which was used for calibrating the charging effects (Fig. 4e).

The surface morphology of pure B–TiO_2, GO and 2GO@B–TiO_2 nanocomposite was analyzed by FIB-SEM (Fig. 5). The white arrows in Fig. 5c evidence TiO_2 particles both in dispersed and aggregated form.

3.2. Evaluation of photocatalytic activity of nanocomposites

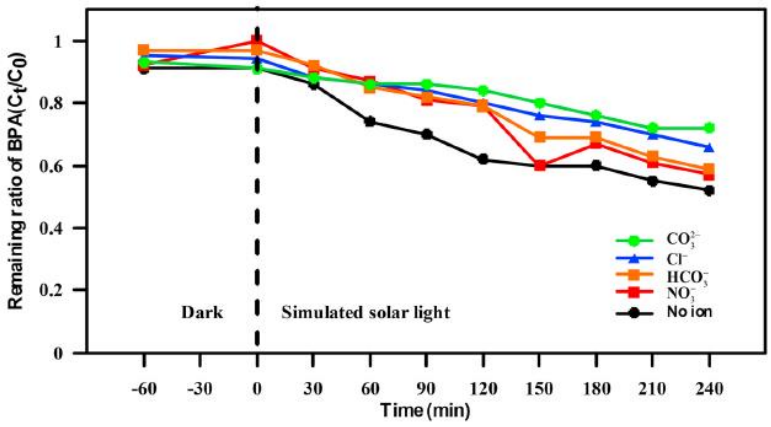
In order to evaluate the photocatalytic performance of the synthesized B–TiO_2 and GO@B–TiO_2, BPA was used as a model organic pollutant in aqueous solution and its degradation was followed under the simulated solar light at ambient conditions. Control experiments (in the dark and without photocatalysts to evaluate BPA photolysis) were carried out under the same conditions. The effect of GO amount on the photocatalytic abilities of the GO@B–TiO_2 nanocomposites was evaluated. As illustrated in Fig. 6a, the adsorption removal efficiencies of BPA over the B–TiO_2, 0.5GO@B–TiO_2, 1GO@B–TiO_2, 2GO@B–TiO_2, 5GO@B–TiO_2 (experiments in the dark) were 5.30%, 8.30%, 9.02%, 12.00% and 1.63%, respectively. The maximum removal percentage by adsorption was obtained for 2GO@B–TiO_2 sample (12.00%). Compared to the B–TiO_2 photocatalyst, the graphene-supported boron doped TiO_2 exhibited higher adsorption ability, probably because GO allows increasing the specific surface area of the composite materials (the nominal specific surface area of GO is ~2600 $m^2\ g^{-1}$) favoring the interaction with the BPA molecules. Nevertheless, when the amount of GO increases too much (i.e. in the presence of 5GO@B–TiO_2), the hydrophilicity of the GO layers surrounding the B–TiO_2 nanoparticles, repulses the hydrophobic BPA molecules hampering an efficient interaction via adsorption.

Fig. 6a shows the catalytic activities of prepared photocatalyst in BPA degradation by means of simulated solar-light driven photocatalysis. BPA is known to be almost recalcitrant to degradation: only 8.10% photolysis in 4 h, but the degradation ratio increased significantly in the presence of the catalysts. After 240 min of irradiation, the degradation of BPA with 2GO@B–TiO_2 (47.66%) is higher than that reached with pure B–TiO_2 (18.78%). The photocatalytic degradation of BPA as a function of irradiation time in the presence of 0.5GO@B–TiO_2, 1GO@B–TiO_2, 2GO@B–TiO_2, 5GO@B–TiO_2 and B–TiO_2 was observed to follow the pseudo first order degradation kinetic law (Fig. 6b and c) and the kinetic constant values were summarized in Table 1. These values have the same magnitude but they are lower than the kinetic constants reported in literature for the degradation of BPA by the benchmark P25 (Evonik, Essen, Germany) TiO_2 photocatalyst under simulated solar light [54–56] Nevertheless, the trend of the kinetic constants of the new photocatalysts follows the trend observed for the adsorption (it increases from 0.5GO@B–TiO_2 up to 2GO@B–TiO_2, then decreases, the smallest value obtained for B–TiO_2 sample), indicating an important role played by the direct interaction photocatalyst-substrate occurring at the material surface via adsorption. Moreover, the photocatalytic activity is strongly influenced by: i) B doping and ii) graphene oxide presence. For what concerns the foster point, it was reported that the B doping into TiO_2 can enhance BPA photodegradation since the recombination of the electron-hole species formed by the hybrid are better hampered than neat TiO_2 under irradiation [57]. For the latter point, as observed in Fig. 1, GO modifies the B–TiO_2 band gap (the electron rich two dimensional π-conjugated graphene oxide suppresses electron/hole recombination events due to its good electron conductivity [57]). The band gap of 3.10 eV observed for B–TiO_2 sample becomes 3.02 eV for the 2GO@B–TiO_2: this allows a more efficient interaction of the material with the visible part of the solar light. Finally, the decrease of photocatalytic activity shown by 5GO@B–TiO_2 sample can also be explained considering that the light cannot penetrate easily through the GO sheets and cannot activate properly the formation of reactive species by B–TiO_2 [58].

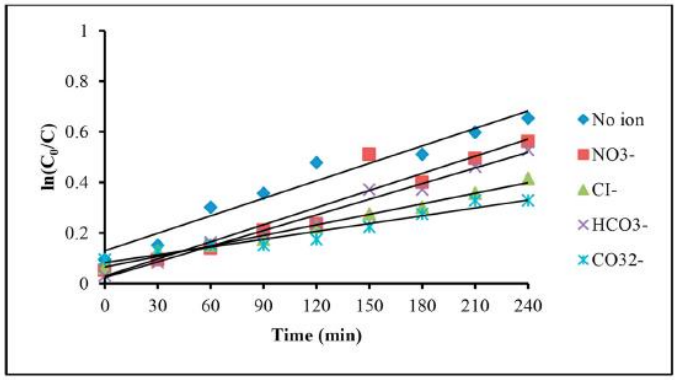
The reaction solution pH has a moderate effect on the adsorption of BPA to the surface of the catalyst. The point of zero charge (pH_{pzc}) value of GO@B–TiO_2 was reported as 6.2 and catalyst surface is positively charged at $pH < pH_{pzc}$, whereas it is negatively charged at $pH > pH_{pzc}$ [53,59]. In aqueous solutions, BPA is present in several forms, namely, undissociated molecules (BPA), $HBPA^-$ and BPA^{2-}, with pKa_1 and pKa_2 values of 9.6 and 10.2, respectively [60]. Basing on these information, the appropriate pH for an effective BPA degradation with GO@B–TiO_2 is expected to be around pH 5, as BPA is undissociated and not charged, whereas the catalyst (the pH is slightly lower than pH_{pzc}) is only slightly positive, so the interaction can occur easily. At higher pHs the interaction (negative BPA form-negatively charged photocatalysts and GO) becomes repulsive, at pH lower than 5 the materials become more and more positive and the interaction with the non-charged molecule decreases as well. Therefore, all experiments were performed at pH 5.

3.2.1. Effect of water matrix

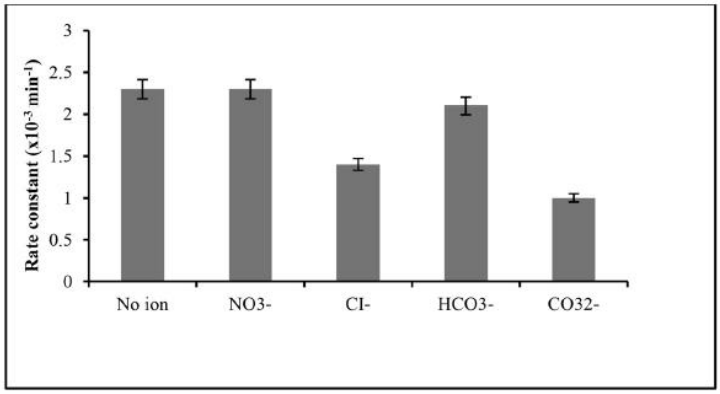
Since widespread inorganic ions such as nitrate, chloride, carbonate and bicarbonate (C_o: 2 mM for all anions) are found in natural water bodies, the effect of these ions on the photocataytic degradation of BPA was investigated. For the sake of simplicity, only the effect on the best photocatalyst (2GO@B–TiO_2) was considered. Fig. 7 shows the anions cause different inhibitory effects on the degradation of BPA. The lack of activity follows the order of carbonate ~ chloride > bicarbonate ~ nitrate. After 4 h of simulated solar light irradiation the corresponding photocatalytic degradation efficiencies became 28.30%, 33.68%, 40.87% and 42.70%, respectively, starting from 47.66%. Their corresponding k values are compared in Table 1S. The more plausible explanation for this behavior may be that the anions have been converted into radical forms less reactive than the hydroxyl radical, and they hampered the adsorption of BPA by occupying the positive charge catalyst surface [61]. Also, these anions could act as a scavenger for hydroxyl radicals. Therefore, the degradation of BPA will be restricted in the presence of the anions. Their effects on photocatalytic degradation can be associated with specific conditions such as the reaction system,



a)

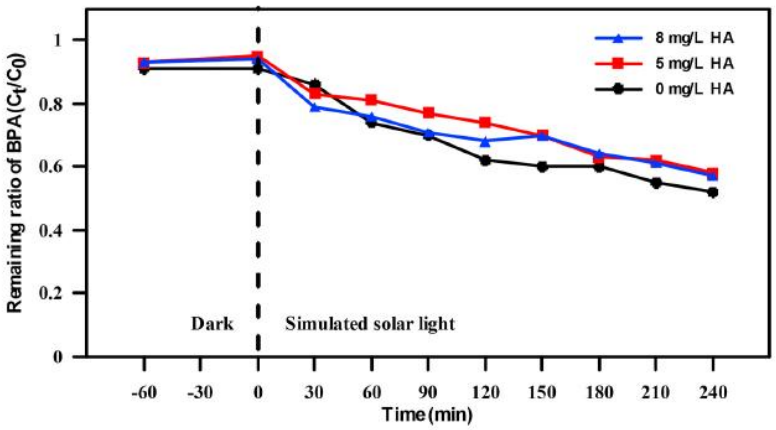


b)

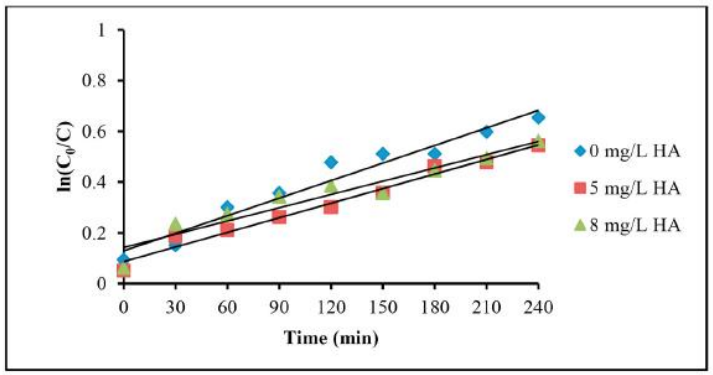


c)

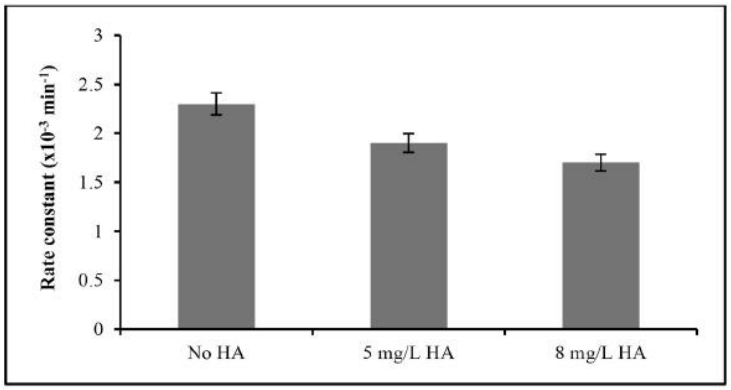
Fig. 7. a) Effect of inorganic anions on BPA degradation, b) relation between ln (C_0/C) and time and c) apparent first-order rate constant (k_{app}) [C_0 = 10 mg L^{-1}; 2GO@B–TiO_2 = 1 g L^{-1}].



a)



b)



c)

Fig. 8. a) Photocatalytic removal of BPA in the presence of different concentrations of HA under solar irradiation, b) relation between ln (C_0/C) and time and c) apparent first-order rate constant (k_{app}) [C_0 = 10 mg L^{-1}; 2GO@B–TiO_2 = 1 g L^{-1}].

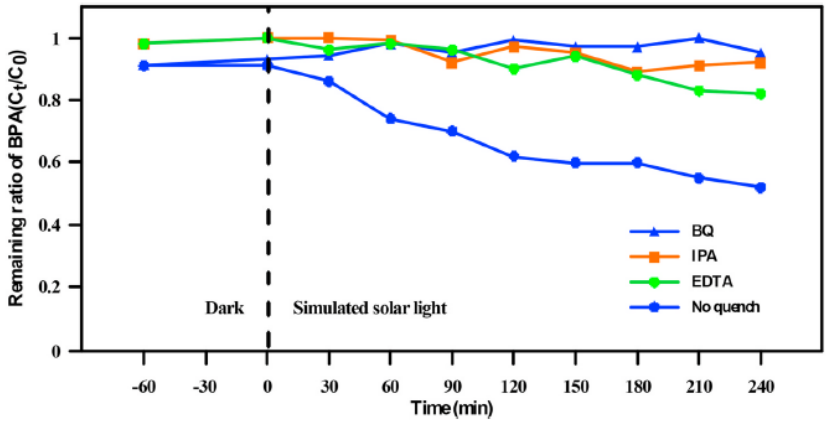


Fig. 9. Comparison of the photocatalytic BPA degradation activities of the 2GO@B–TiO_2 photocatalyst in the presence of different scavengers, [C_0 = 10 mg L^{-1}; 2GO@B–TiO_2 = 1 g L^{-1}].

the type of pollutant and the type of the photocatalyts, and so on [62].

Humic acid (HA) solution was also used to simulate real natural water. HA is an important natural organic component (NOM), typically present in surface water, and negatively affecting the physical and chemical reactions expected during the Advanced Oxidation processes due to important interferences with the ROS (Reactive Oxygen Species formed during the photocatalytic processes). Considering that the concentration of HA usually varies from 2 to 10 mg L^{-1} in surface natural water, 5 or 8 mg L^{-1} HA were added to the reaction solution [63]. As shown in Fig. 8, the presence of HA in the reaction solution slightly affected the photocatalytic degradation of BPA. In detail, when the reaction solution is spiked with 8 mg L^{-1} HA and 5 mg L^{-1} HA, BPA degradation rate decreased from 47.66% to 41.86% and 43.33%, respectively (the corresponding k values are shown in Table 1S). The slight activity decrease could be due to: (i) the competitive adsorption of HA with BPA on the surface of the catalyst that retards the photocatalytic oxidation process interfering with the ROS, and (ii) the decrease of light penetration in the suspension. Based on the above experimental results containing both ions and HA, photocatalytic degradation of BPA is expected to be slower in real water samples [64].

3.2.2. Detection of the reactive species

To determine ROS during the degradation process, experiments with proper scavenging agents were performed over the 2GO@B–TiO_2 catalyst applying the same experimental conditions described above. The addition of BZQ causes the capture of active $O_2^{\cdot-}$ radicals, the addition of IPA and EDTA causes the elimination of $^{\cdot}OH$ and h^+. As it can be seen in Fig. 9, the three scavengers affect significantly the BPA degradation extent. The values of k and photocatalytic degradation percentages are summarized in Table 1S. They indicate that all three radicals contribute to the photocatalytic activity of 2GO@B–TiO_2 in the order $O_2^{\cdot-}$ > OH > h^+.

$^{\cdot}OH$ radical species generation during the reaction process of 2GO@B–TiO_2 and B–TiO_2 was further investigated using the PL probing technique. As shown in Fig. 10, the PL emission signal in the presence of 2GO@B–TiO_2 increased significantly increasing the irradiation time with respect to B–TiO_2 catalyst. The result indicates that $^{\cdot}OH$ species were produced under simulated solar light irradiation, but the generation is faster and more efficient in the presence of 2GO@B–TiO_2 composite.

According to the observed results, it can be inferred that the photocatalytic reaction process of BPA with 2GO@B–TiO_2 under simulated solar light irradiation can occur as follows Eqs (3)–(7) [34] and Scheme 3 and Eqs. (3)–(7) indicate our suggested mechanism for degradation of BPA under simulated solar light.

$$GO@B\text{–}TiO_2 + hv\ (solar\ light) \rightarrow e^-_{(CB)} + h^+_{(VB)} \quad (3)$$

$$CB\ (e^-) + O_2 \rightarrow O_2^{\cdot-} \quad (4)$$

$$O_2^{\cdot-} + 2H^+ + CB\ (e^-) \rightarrow H_2O_2 \quad (5)$$

$$H_2O_2 + CB\ (e^-) \rightarrow OH^- + OH \quad (6)$$

$$BPA + ROS \rightarrow \text{by products} \quad (7)$$

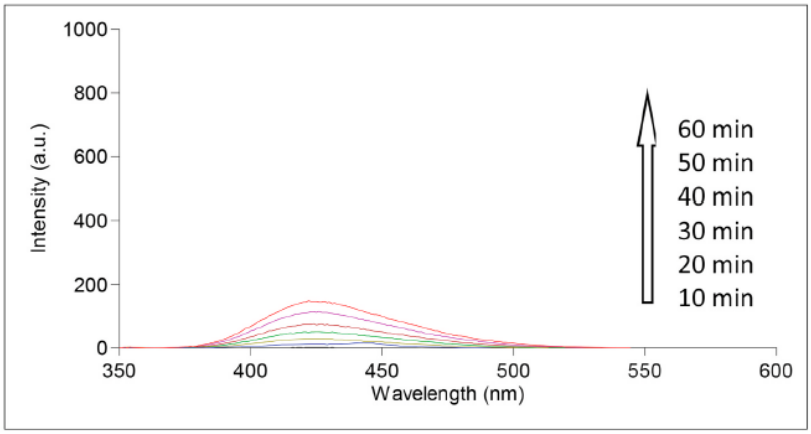
3.2.3. Photocatalytic reusability experiments

Besides the photocatalytic activity, re-use efficiency of the catalyst was studied in view of a transfer on a large scale of the photocatalytic operation in water purification technologies. The reusability test of the 2GO@B–TiO_2 was performed and the degradation/adsorption removal of BPA monitored along five successive experiments under simulated solar light irradiation. After each BPA photocatalytic experiment (240 min), the catalyst was collected after centrifugation and washed with water. The solid was left to dry at 80 °C overnight and then reused in a new experiment in the same conditions. The degradation/adsorption efficiency results obtained after 5 cyles are displayed in Fig. 11. In the second usage, the activity of the catalyst was slightly reduced, probably because the by-products produced during the BPA degradation remained adsorbed at the catalyst surface despite washing. Nevertheless, higher degradation activities were obtained in the following cycles, probably because the adsorbed by-products were degraded for the prolonged irradiation. In conclusion, 2GO@B–TiO_2 nanocomposite was effective for use in consecutive runs.

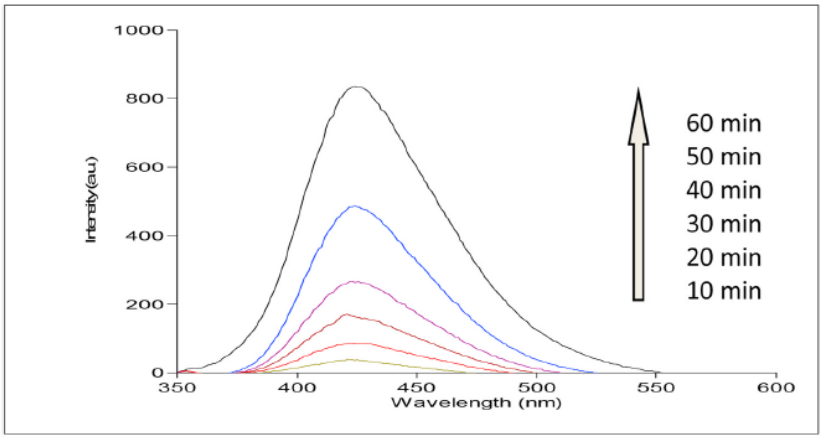
After the photocatalytic tests, 2GO@B–TiO_2 catalyst was submitted to new XRD and Raman analyses (Figs. 1S and 2S, respectively). The crystal phase and the Raman behaviors of the catalyst were not modified, indicating that the hybrid catalyst was stable during and after the photocatalytic action.

4. Conclusions

In conclusion, GO@B–TiO_2 nanocomposites were prepared using a two-step procedure, to produce improved B–TiO_2-based photocatalysts.



a)



b)

Fig. 10. a) ·OH trapping PL spectra of B–TiO_2 and b) 2GO@B–TiO_2 in TA solution upon simulated solar light exposure.

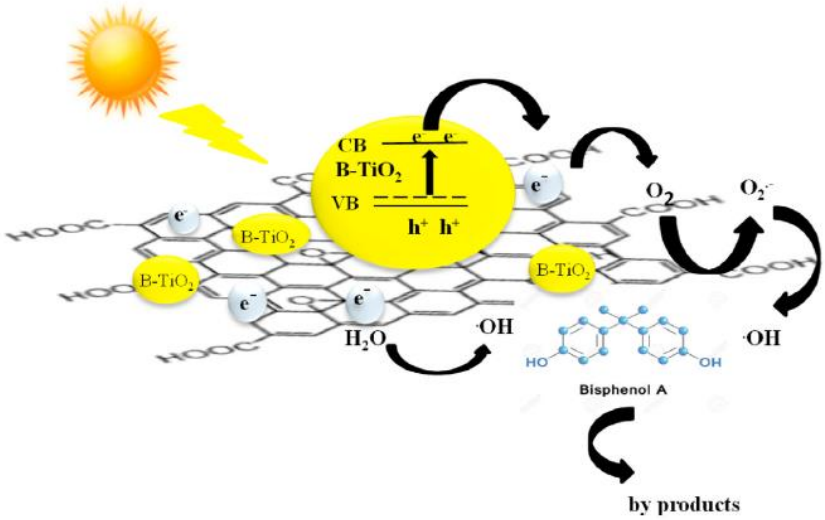
Several physicochemical techniques were applied to clarify structure and morphology of the nanocomposites. Among the others, 2GO@B–TiO_2 system demonstrated an enhanced efficiency towards BPA photocatalytic degradation. The inhibitory effect of inorganic anions on the photocatalytic performance was in order: $CO_3^{2-} \sim Cl^- > HCO_3^- \sim NO_3^-$. $^{\cdot}O_2^-$ was defined as the primary reactive oxidizing species during the photocatalysis. No significant reduction in the BPA catalytic activity was observed during five cycles in the reusability test, showing that the 2GO@B–TiO_2 catalyst remains stable and performance in time and can be applied in scale-up processes. The present study could be a useful basis for field-based testing and applicability of solar light photocatalyst technology for the treatment of wastewater especially those containing endocrine-disrupting compounds.

CRediT authorship contribution statement

Ilknur Altin: Material synthesis, Photocatalytic tests, Investigation, Formal analysis, Writing - original draft, Visualization. **Xianzheng Ma:** Material synthesis, Investigation, Formal analysis. **Vittorio Boffa:** Conceptualization, Methodology, Resources, Writing - review & editing, Supervision. **Emin Bacaksız:** Characterization, Formal analysis, Writing - review & editing. **Giuliana Magnacca:** Characterization, Formal analysis, Writing - review & editing.

Declaration of competing interest

The authors declare that they have no known competing financial interests or personal relationships that could have appeared to influence the work reported in this paper.



Scheme 3. The mechanism proposed for BPA degradation in the presence of GO@B–TiO_2.

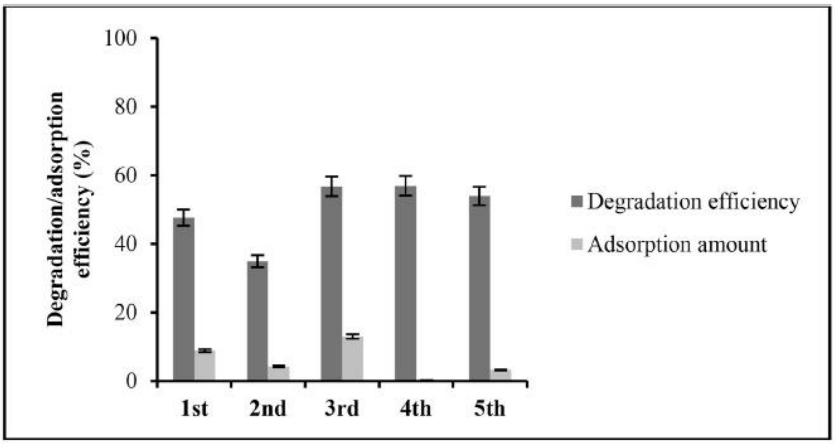


Fig. 11. The recycling tests of 2GO@B–TiO_2 [C_0 = 10 mg L^{-1}; 2GO@B–TiO_2 = 1 g L^{-1}].

References

[1] S. Vadivel, N. Naveen, V.P. Kamalakannan, P. Cao, N. Balasubramanian, Facile large scale synthesis of Bi_2S_3 nano rods–graphene composite for photocatalytic photoelectrochemical and supercapacitor application, Appl. Surf. Sci. 351 (2015) 635–645, https://doi.org/10.1016/j.apsusc.2015.04.101.

[2] M.V. Liga, E.L. Bryant, V.L. Colvin, Q. Li, Virus inactivation by silver doped titanium dioxidenanoparticles for drinking water treatment, Water Res. 45 (2011) 535–544, https://doi.org/10.1016/j.watres.2010.09.012.

[3] Y. Zhang, J.L. Zhou, Occurrence and Removal of Endocrine Disrupting Chemicals in Wastewater, vol. 73, 2008, pp. 848–853, https://doi.org/10.1016/j.chemosphere.2008.06.001.

[4] T. Deblonde, C. Cossu-Leguille, P. Hartemann, Emerging pollutants in wastewater: a review of the literatüre, Int. J. Hyg Environ. Health 214 (2011) 442–448, https://doi.org/10.1016/j.ijheh.2011.08.002.

[5] M. Giulivo, M. Lopez de Alda, E. Capri, D. Barcelo, Human exposure to endocrine disrupting compounds: their role in reproductive systems, metabolic syndrome and breast cancer, A review, Environ. Res. 151 (2016) 251–264, https://doi.org/10.1016/j.envres.2016.07.011.

[6] V. Belgiorno, L. Rizzo, D. Fatta, C. Della Rocca, G. Lofrano, A. Nikolaou, V. Naddeo, S. Meric, Review on endocrine disrupting-emerging compounds in urban wastewater: occurrence and removal by photocatalysis and ultrasonic irradiation for wastewater reuse, Desalination 215 (2007) 166–176, https://doi.org/10.1016/j.desal.2006.10.035.

[7] J. Michałowicz, Bisphenol A–Sources, toxicity and biotransformation, Environ. Toxicol. Pharmacol. 37 (2014) 738–758, https://doi.org/10.1016/j.etap.2014.02.003.

[8] R. Asahi, T. Morikawa, T. Ohwaki, K. Aoki, Y. Taga, Visible-light photocatalysis in nitrogen-doped titanium oxides, Science 293 (2001) 269–271, https://doi.org/10.1126/science.1061051.

[9] Z. Yi, J. Ye, N. Kikugawa, T. Kako, S. Ouyang, H. Stuart-Williams, H. Yang, J. Cao, W. Luo, Z. Li, Y. Liu, R.L. Withers, An orthophosphate semiconductor with photooxidation properties under visible-light irradiation, Nat. Mater. 9 (2010) 559–564, https://doi.org/10.1038/nmat2780.

[10] S. Banerjee, S.C. Pillai, P. Falaras, K.E. O'Shea, J.A. Byrne, D.D. Dionysiou, New insights into the mechanism of visible light photocatalysis, J. Phys. Chem. Lett. 5 (2014) 2543–2554, https://doi.org/10.1021/jz501030x.

[11] L.V. Bora, R.K. Mewada, Visible/solar light active photocatalysts for organic effluent treatment: fundamentals, mechanisms and parametric review, Renew. Sustain. Energy Rev. 76 (2017) 1393–1421, https://doi.org/10.1016/j.rser.2017.01.130.

[12] W.W. Anku, S.O.B. Oppong, S.K. Shukla, E.S. Agorku, P.P. Govender, Palladium-doped–ZrO_2–multiwalled carbon nanotubes nanocomposite: an advanced photocatalyst for water treatment, Appl. Phys. A 122 (2016) 579, https://doi.org/10.1007/s00339-016-0086-8.

[13] S.O.B. Oppong, W.W. Anku, S.K. Shukla, P.P. Govender, Lanthanum doped–TiO_2 decorated on graphene oxide nanocomposite: a photocatalyst for enhanced degradation of acid blue 40 under simulated solar light, Adv. Mater. Lett. 8 (3) (2017) 295–302, https://doi.org/10.5185/amlett.2017.6826.

[14] W.W. Anku, S.O.B. Oppong, S.K. Shukla, P.P. Govender, Influence of ZnO concentration on the optical and photocatalytic properties of Ni-doped ZnS/ZnO nanocomposite, Bull. Mater. Sci. 39 (2016) 1745–1752, https://doi.org/10.1007/s12034-016-1310-z.

[15] I. Altın, M. Sökmen, Preparation of TiO_2-polystyrene photocatalyst from waste material and its usability for removal of various pollutants, Appl. Catal., B 144 (2014) 694–701, https://doi.org/10.1016/j.apcatb.2013.06.014.

[16] B. Chen, J. Hou, K. Lu, Formation mechanism of TiO_2 nanotubes and their applications in photoelectrochemical water splitting and supercapacitors, Langmuir 29 (19) (2013) 5911–5919, https://doi.org/10.1021/la400586r.

[17] Y. Zhang, P. Xiao, X. Zhou, D. Liu, B. Batalla Garcia, G. Cao, Carbon monoxide annealed TiO_2 nanotube array electrodes for efficient biosensor applications, J. Mater. Chem. 19 (7) (2009) 948–953, https://doi.org/10.1039/B818620K.

[18] X. Bai, L. Yang, A. Hagfeldt, E.M.J. Johansson, P. Jin, D35-TiO_2 nano-crystalline film as a high performance visible-light photocatalyst towards the degradation of *bis*-phenol A, Chem. Eng. J. 355 (2019) 999–1010, https://doi.org/10.1016/j.cej.2018.08.061.

[19] H. Guo, H. Wang, Q. Wu, J. Li, Degradation and mechanism analysis of bisphenol A in aqueous solutions by pulsed discharge plasma combined with activated carbon, Separ. Purif. Technol. 190 (2018) 288–296, https://doi.org/10.1016/j.seppur.2017.09.002.

[20] K. Davididou, R. Nelson, J.M. Monteagudo, A. Duran, A.J. Exposito, E. Chatzisymeon, Photocatalytic degradation of bisphenol-A under UV-LED, blacklight and solar irradiation, J. Clean. Prod. 203 (2018) 13–21, https://doi.org/10.1016/j.jclepro.2018.08.247.

[21] L. Xu, L. Yang, E.M.J. Johansson, Y. Wang, P. Jin, Photocatalytic activity and mechanism of bisphenol a removal over TiO_2−x/rGO nanocomposite driven by visible light, Chem. Eng. J. 350 (2018) 1043–1055, https://doi.org/10.1016/j.cej.2018.06.046.

[22] M. Salari, K. Konstantinov, H. Kun Liu, Enhancement of the capacitance in TiO_2 nanotubes through controlled introduction of oxygen vacancies, J. Mater. Chem. 21 (13) (2011) 5128–5133, https://doi.org/10.1039/C0JM04085A.

[23] X. Chen, L. Liu, Y. Yu Peter, S.S. Mao, Increasing solar absorption for photocatalysis with black hydrogenated titanium dioxide nanocrystals, Science 331 (6018) (2011) 746–750, https://doi.org/10.1126/science.1200448.

[24] A. Mattsson, M. Leideborg, K. Larsson, G. Westin, L. Österlund, Adsorption and solar light decomposition of acetone on anatase TiO_2 and niobium doped TiO_2 thin films, J. Phys. Chem. B 110 (3) (2006) 1210–1220, https://doi.org/10.1021/jp055656z.

[25] A. Kudo, Y. Miseki, Heterogeneous photocatalyst materials for water splitting, Chem. Soc. Rev. 38 (2009) 253–278, https://doi.org/10.1039/B800489G.

[26] M. Li, S.F. Zhou, Y.W. Zhang, G.Q. Chen, Z.L. Hong, One-step solvothermal preparation of TiO_2/C composites and their visible-light photocatalytic activities, Appl. Surf. Sci. 254 (2008) 3762–3766, https://doi.org/10.1016/j.apsusc.2007.11.047.

[27] C.H. Choi, M.W. Chung, H.C. Kwon, S.H. Park, S.I. Woo, B, N- and P, N-doped graphene as highly active catalysts for oxygen reduction reactions in acidic media, J. Mater. Chem. A 1 (2013) 3694–3699, https://doi.org/10.1039/C3TA01648J.

[28] H. Dong, G. Zeng, L. Tang, C. Fan, C. Zhang, X. He, Y. He, An overview on limitations of TiO_2-based particles for photocatalytic degradation of organic pollutants and the corresponding countermeasures, Water Res. 79 (2015) 128–146, https://doi.org/10.1016/j.watres.2015.04.038.

[29] L.K. Putri, W.-J. Ong, W.S. Chang, S.-P. Chai, Heteroatom doped graphene in photocatalysis: a review, Appl. Surf. Sci. 358 (2015) 2–14, https://doi.org/10.1016/j.apsusc.2015.08.177.

[30] N. Khalid, E. Ahmed, Z. Hong, Y. Zhang, M. Ahmad, Nitrogen doped TiO_2 nanoparticles decorated on graphene sheets for photocatalysis applications, Curr. Appl. Phys. 12 (2012) 1485–1492, https://doi.org/10.1016/j.cap.2012.04.019.

[31] W. Li, Y. Bai, W. Zhuang, K.Y. Chan, C. Liu, Z. Yang, X. Feng, X. Lu, Highly crystalline mesoporous TiO_2(B) nanofibers, J. Phys. Chem. C 118 (2014) 3049–3055, https://doi.org/10.1021/jp408112z.

[32] V.H. Luan, H.N. Tien, S.H. Hur, Fabrication of 3D structured ZnO nanorod/reduced graphene oxide hydrogels and their use for photo-enhanced organic dye removal, J. Colloid Interface Sci. 437 (2015) 181–186, https://doi.org/10.1016/j.jcis.2014.08.071.

[33] X. Bai, X. Huang, X.Y. Zhang, Z.L. Hua, C.F. Wang, Q. Qin, Q. Zhang, TiO_2–graphene nanoparticle based electrochemical sensor for the bimodal-response detection of 4-chlorophenol, RSC Adv. 4 (2014) 13461–13468, https://doi.org/10.1039/C3RA48065H.

[34] H. Wu, J. Fan, E. Liu, X. Hu, Y. Ma, X. Fan, Y. Li, C. Tang, Facile hydrothermal synthesis of TiO_2 nanospindles-reduced graphene oxide composite with an enhanced photocatalytic activity, J. Alloys Compd. 623 (2015) 298–303, https://doi.org/10.1016/j.jallcom.2014.10.153.

[35] N.J. Bell, Y.H. Ng, A. Du, H. Coster, S.C. Smith, R. Amal, Understanding the enhancement in photoelectrochemical properties of photocatalytically prepared TiO_2-reduced graphene oxide composite, J. Phys. Chem. C 115 (2011) 6004–6009, https://doi.org/10.1021/jp1113575.

[36] A. Du, Y.H. Ng, N.J. Bell, Z. Zhu, R. Amal, S.C. Smith, Hybrid graphene/titania nanocomposite: interface charge transfer, hole doping, and sensitization for visible light response, J. Phys. Chem. Lett. 2 (2011) 894–899, https://doi.org/10.1021/jz2002698.

[37] W. Han, L. Chen, W. Song, S. Wang, X. Fan, Y. Li, F. Zhang, G. Zhang, W. Peng, Synthesis of nitrogen and sulfur co-doped reduced graphene oxide as efficient metal-free cocatalyst for the photo-activity enhancement of CdS, Appl. Catal., B 236 (2018) 212–221, https://doi.org/10.1016/j.apcatb.2018.05.021.

[38] L. Xu, L. Yang, E.M.J. Johansson, Y. Wang, P. Jin, Photocatalytic activity and mechanism of bisphenol a removal over TiO_2−x/rGO nanocomposite driven by visible light, Chem. Eng. J. 350 (2018) 1043–1055, https://doi.org/10.1016/j.cej.2018.06.046.

[39] E. Piera, M.I. Tejedor-Tejedor, M.E. Zorn, M.A. Anderson, Relationship concerning the nature and concentration of Fe(III) species on the surface of TiO_2 particles and photocatalytic activity of the catalyst, Appl. Catal., B 46 (2003) 671–685, https://doi.org/10.1016/S0926-3373(03)00288-1.

[40] W. Lv, D. Tang, Y. He, C. You, Z. Shi, X. Chen, Low-temperature exfoliated graphenes: vacuum-promoted exfoliation and electrochemical energy storage, ACS Nano 3 (2009) 3730–3736, https://doi.org/10.1021/nn900933u.

[41] W.S. Hummers, R.E. Offeman, Preparation of graphitic oxide, J. Am. Chem. Soc. 80 (1958), https://doi.org/10.1021/ja01539a017, 1339-1339.

[42] A. Taufika, A. Alberta, R. Saleh, Sol-gel synthesis of ternary CuO/TiO_2/ZnO nanocomposites for enhanced photocatalytic performance under UV and visible light irradiation, J. Photochem. Photobiol., A 344 (2017) 149–162, https://doi.org/10.1016/j.jphotochem.2017.05.012.

[43] H. Safardoust-Hojaghan, M. Salavati-Niasari, Degradation of methylene blue as a pollutant with N-doped graphene quantum dot/titanium dioxide nanocomposite, J. Clean. Prod. 148 (2017) 31–36, https://doi.org/10.1016/j.jclepro.2017.01.169.

[44] S.D. Perera, R.G. Mariano, K. Vu, N. Nour, O. Seitz, Y. Chabal, K.J. Balkus, Hydrothermal synthesis of graphene-TiO_2 nanotube composites with enhanced photocatalytic activity, ACS Catal. 2 (2012) 949–956, https://doi.org/10.1021/cs200621c.

[45] P. Wang, J. Wang, X. Wang, H. Yu, J. Yu, M. Lei, Y. Wang, One-step synthesis of easy-recycling TiO_2-rGO nanocomposite photocatalysts with enhanced photocatalytic activity, Appl. Catal., B 132–133 (2013) 452–459, https://doi.org/10.1016/j.apcatb.2012.12.009.

[46] R. Rao, R. Podila, R. Tsuchikawa, J. Katoch, D. Tishler, A. Rao, M. Ishigami, Effects of layer stacking on the combination Raman modes in graphene, ACS Nano 5 (2011) 1594–1599, https://doi.org/10.1021/nn1031017.

[47] M. Cao, P. Wang, Y. Ao, W. Chao, J. Hou, Q. Jin, Photocatalytic degradation of tetrabromobisphenol A by a magnetically separable graphene–TiO_2 composite photocatalyst: mechanism and intermediates analysis, Chem. Eng. J. 264 (2015) 113–124, https://doi.org/10.1016/j.cej.2014.10.011.

[48] Q. Chen, H. Liu, Y. Xin, X. Cheng, TiO_2 nanobelts–Effect of calcination temperature on optical, photoelectrochemical and photocatalytic properties, Electrochim. Acta 111 (2013) 284–291, https://doi.org/10.1016/j.electacta.2013.08.049.

[49] Wenjie Zhang, Bo Yang, Jinlei Chen, Effects of calcination temperature on preparation of boron-doped TiO2 by sol-gel method, Int J Photoenergy, 2012. Article ID 528637, https://doi:10.1155/2012/528637.

[50] N. Feng, A.M. Zheng, Q. Wang, et al., Boron environments in B-doped and (B, N) codoped TiO_2 photocatalysts: a combined solid-state NMR and theoretical calculation study, J. Phys. Chem. C 115 (2011) 2709–2719, https://doi.org/10.1021/jp108008a.

[51] D.H. Quiñones, A. Rey, P.M. Álvarez, F.J. Beltrán, G. Li Puma, Boron doped TiO2 catalysts for photocatalytic ozonation of aqueous mixtures of common pesticides: diuron, o-phenylphenol, MCPA and terbuthylazine, Appl. Catal., B 178 (2015) 74–81, https://doi.org/10.1016/j.apcatb.2014.10.036.

[52] Y.L. Su, X.W. Zhang, S. Han, X.Q. Chen, L.C. Lei, F-B-codoping of anodized TiO_2 nanotubes using chemical vapor deposition, Electrochem. Commun. 9 (2007) 2291–2298, https://doi.org/10.1016/j.elecom.2007.06.038.

[53] X. Fan, G. Zhang, F. Zhang, Multiple roles of graphene in heterogeneous catalysis, Chem. Soc. Rev. 44 (2015) 3023–3035, https://doi.org/10.1039/C5CS00094G.

[54] A. Garg, T. Singhania, A. Singh, S. Sharma, S. Rani, A. Neogy, S.R. Yadav, V. K. Sangal, N. Garg, Photocatalytic degradation of bisphenol-A using N, Co codoped TiO_2 catalyst under solar light, Sci. Rep. 9 (2019) 765, https://doi.org/10.1038/s41598-018-38358-w.

[55] V.M. Mboula, V. Hequet, Y. Andrès, L.M. Pastrana-Martinez, J.M. Don˜a-Rodriguez, A.M.T. Silva, P. Falaras, Photocatalytic degradation of endocrine disruptor compounds under simulated solar light, Water Res. 47 (2013) 3997–4005, https://doi.org/10.1016/j.watres.2013.01.055.

[56] H. Dimitroula, V.M. Daskalaki, Z. Frontistis, D.I. Kondarides, P. Panagiotopoulou, N.P. Xekoukoulotakis, D. Mantzavinos, Solar photocatalysis for the abatement of emerging micro-contaminants in wastewater: synthesis, characterization and testing of various TiO_2 samples, Appl. Catal. B Environ. 117–118 (2012) 283–291, https://doi.org/10.1016/j.apcatb.2012.01.024.

[57] D.M. Chen, D. Yang, Q. Wang, Z.Y. Jiang, Effects of boron doping on photocatalytic activity and microstructure of titanium dioxide nanoparticles, Ind. Eng. Chem. Res. 45 (2006) 4110–4116, https://doi.org/10.1021/ie0600902.

[58] J. Pan, X. Zhang, A. Du, D. Sun, J.O. Leckie, Self-etching reconstruction of hierarchically mesoporous F-TiO_2 hollow microspherical photocatalyst for

concurrent membrane water purifications, J. Am. Chem. Soc. 130 (2008) 11256–11257, https://doi.org/10.1021/ja803582m.
[59] I.V. Lightcap, T.H. Kosel, P.V. Kamat, Anchoring semiconductor and metal nanoparticles on a two-dimensional catalyst mat. Storing and shuttling electrons with reduced graphene oxide, Nano Lett. 10 (2010) 577–583, https://doi.org/10.1021/nl9035109.
[60] J. Xu, L. Wang, Y. Zhu, Decontamination of bisphenol A from aqueous solution by graphene adsorption, Langmuir 28 (2012) 8418–8425, https://doi.org/10.1021/la301476p.
[61] X. Gao, Q. Guo, G. Tang, W. Peng, Y. Luo, D. He, Effects of inorganic ions on the photocatalytic degradation of carbamazepine, Journal of Water Reuse and Desalination (2019) 301–309, https://doi.org/10.2166/wrd.2019.001.
[62] K. Lin, W. Liu, J. Gan, Oxidative removal of bisphenol a by manganese dioxide: efficacy, products, and pathways, Environ. Sci. Technol. 43 (2009) 3860–3864, https://doi.org/10.1021/es900235f.
[63] C. Wang, L. Zhu, M. Wei, P. Chen, G. Shan, Photolytic reaction mechanism and impacts of coexisting substances on photodegradation of bisphenol A by Bi_2WO_6 in water, Water Res. 46 (2012) 845–853, https://doi.org/10.1016/j.watres.2011.11.057.
[64] M. Antonopoulou, C.G. Skoutelis, C. Daikopoulos, Y. Deligiannakis, I. K. Konstantinou, Probing the photolyticephotocatalytic degradation mechanism of DEET in the presence of natural or synthetic humic macromolecules using molecular-scavenging techniques and EPR spectroscopy, J. Environ. Chem. Eng. 3 (2015) 3005–3014, https://doi.org/10.1016/j.jece.2015.02.020.